Received 20 September 2023; accepted 12 October 2023. Date of publication 18 October 2023; date of current version 1 November 2023.
The review of this article was arranged by Editor A. Nathan.

*Digital Object Identifier 10.1109/JEDS.2023.3325465*

# A 121 A/cm$^2$ High Current Density Copolymer OSC-Based Thin-Film Power OFET With 300 V Off-State Breakdown Voltage

**FUBIN WANG[1,2], JUN ZHANG[1,2] (Member, IEEE), HAO ZHANG[1,2], LEI WANG[1,2], XIN WU[1,2], HAONAN LIN[1,2], JIAYI ZHOU[1,2], YUHAO WANG[1,2], JIAFEI YAO[1,2] (Member, IEEE), JING CHEN[1,2], KEMENG YANG[1,2], MAN LI[1,2], AND YUFENG GUO[1,2] (Member, IEEE)**

1 College of Integrated Circuit Science and Engineering, Nanjing University of Posts and Telecommunications, Nanjing 210046, China
2 National and Local Joint Engineering Laboratory for RF Integration and Micro-Packaging Technologies, Nanjing University of Posts and Telecommunications, Nanjing 210046, China
CORRESPONDING AUTHORS: J. ZHANG and Y. GUO (e-mail: bravaisxx@163.com; yfguo@njupt.edu.cn)

This work was supported in part by the National Natural Science Foundation of China under Grant 62274091; in part by the Jiangsu Association for Science and Technology Youth Science and Technology Talents Lifting Project under Grant TJ-2022-048; and in part by the Natural Science Foundation of Jiangsu Province under Grant BK20201206 and Grant BK20211104.

**ABSTRACT** The long-term absence of organic drive management circuits has prevented organic integration from achieving full flexibility. The high off-state breakdown performance and its avalanche-like breakdown mechanism of copolymer Organic Semiconductor (OSC)-based Organic Field Effect Transistors (OFETs) have been revealed in recent researches. By employing diketopyrrolopyrrole-based conjugated copolymer OSC(DPPT-TT) as the semiconductor layer and Polymethyl methacrylate(PMMA) as the dielectric/passivation layer, the H-bridge circuit can be fabricated with four OFETs integrated on the same Corning glass substrate. The non-destructive avalanche-like breakdown mechanism provides the power OFET a 300 V high BV(Breakdown Voltage), whose critical electric field excesses 5 MV/cm. The fabricated devices also demonstrated the high current density more than 121 A/cm$^2$ and field-effect mobility up to 0.22 cm$^2$/(V·s). The top-gate bottom-contact structure allows the fabricated OFETs a high on-state current density and good device stability without using package construction or other special isolation techniques. By connecting resistors and LEDs on the load side of the H-bridge circuit made of 63 μm channel devices, measurement results show that it has good driving effects and driving performance. These measured results show that organic power devices are a potential candidate for application in the power realm.

**INDEX TERMS** Organic field-effect transistors, conjugated polymer, breakdown voltage (BV), H-bridge circuit, current density.

## I. INTRODUCTION

In the past decade, organic semiconductor(OSC)-based digital and analog integrated circuits(ICs) have been reported for many applications [1], [2], [3], [4]. However, due to the long absence of core organic power transistors with high breakdown voltage(BV), most of the research on organic integrated circuits are based on complementary organic integrated circuits, and the organic power ICs for driving and managing the organic solar cells and batteries have yet to be presented [5], [6]. Recently, the exceptional off-state breakdown performance of copolymer OSCs has been experimentally revealed, and an above 5 MV/cm high critical electric field is achieved by using copolymer OSC-based Schottky junctions [6], [7]. The high breakdown performance of the copolymer-based organic devices creates a new approach to realizing the organic power ICs for future power applications. Although the astonishing avalanche-like breakdown performance of copolymer OSC-based organic field effect transistors(OFETs) has been revealed in recent researches, the copolymer OSC-based power management circuit has not been reported yet [6], [7]. Due to the existence of high-voltage issues with both the drain supply

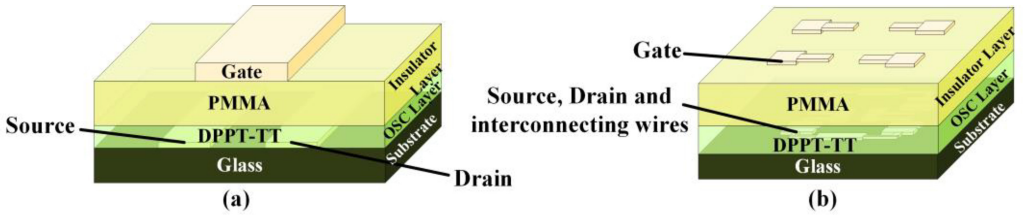


**FIGURE 1.** The 3-D view of the (a) OFET and (b) H-bridge circuit.

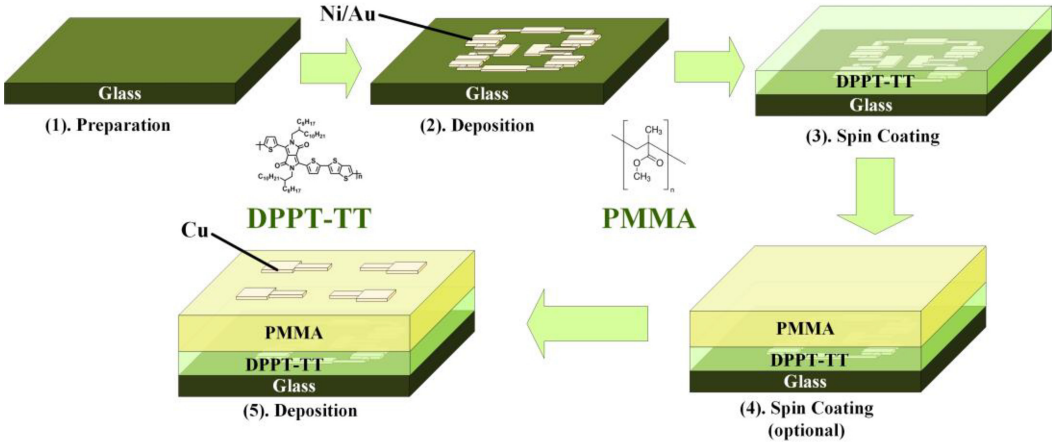


**FIGURE 2.** The fabrication process of H-bridge circuits. (1) Preparation of the substrate. (2) Deposition of Source, Drain and interconnecting wires (Magnetron sputtering, 5nm Ni and 20nm Au). (3) Spin coating of OSC layer (25nm DPPT-TT). (4) Spin coating of Gate Insulator layer (600nm PMMA). (5) Deposition of Gate contact (Magnetron sputtering, 70nm Cu). The inset shows the molecular structure of DPPT-TT and PMMA.

voltage and gate voltage in lateral power devices, the influence of the parasitic transistor and the interference between high-voltage transistors may result in the failure and damage of the whole power management circuit and module. Normally, for silicon-based power ICs, the components that make up the circuit on a monolithic die need to have electrical isolation from each other in order to function. Yet, these electrical isolation techniques, such as mesa isolation, reverse-biased PN junction isolation, oxide isolation, and trench isolation, require valuable area to be implemented, which causes the higher cost and lower integration of power management circuits. However, due to the distinctive electric characteristic of copolymer OSCs, such as ambipolar conduction capability and avalanche-like breakdown mechanism, the above-mentioned isolation structure may not be necessary while maintaining the functionality and performance of the circuit. As a result, the OSC-based power management circuits can be more area- and cost-efficient.

In light of that, by using a simple but reliable solution-based process, thin-film power OFETs with 300 V BV are fabricated to form a simple H-bridge circuit without introducing isolation techniques between devices. Experimental results show that the fabricated OSC-based H-bridge circuits can operate properly without obvious leakage currents between devices. The fabricated device is capable of achieving up to a 121 A/cm$^2$ high current density, a high on-off current ratio(above $10^4$) and field-effect mobility up to 0.22 cm$^2$/(V·s). The fabricated H-bridge circuit and its core devices present good stability and reliability after more than 20 times of repeated BV tests, no damage or degradation caused by thermal breakdown can be observed. The BV tests are conducted within 48 hours. To further explore the driving performance of the device, the fabricated H-bridge circuit is connected in series with a large resistor and an LED lamp on the load side, respectively. The measured results indicate a good on-state driving performance of the fabricated H-bridge circuit composed of thin-film power OFETs.

## II. STRUCTURE, FABRICATION AND MEASUREMENT

As shown in Fig. 1(a) and (b), the core component of the H-bridge circuit, the thin-film lateral power OFET is constructed by employing the diketopyrrolopyrrole-based conjugated copolymer OSC(DPPT-TT) as the semiconductor layer and polymethyl methacrylate(PMMA) as the dielectric/passivation layer respectively.

Due to the organic material nature of DPPT-TT and PMMA, the OSC-based H-bridge circuit is fabricated by using the simple and cost-effective spin-coating technique without introducing high-temperature processes. Fig. 2 shows the fabrication process of the H-bridge circuit. The process flow is composed of four main steps: (1). Fabricating drain and source electrodes: deposit a 5 nm Ni and follow a 20 nm layer of Au to as the drain, source electrodes and interconnecting wires(bottom electrode is patterned using a metal mask covered onto the substrate); (2). Fabricating semiconductor layer: spin coat a layer of DPPT-TT as the

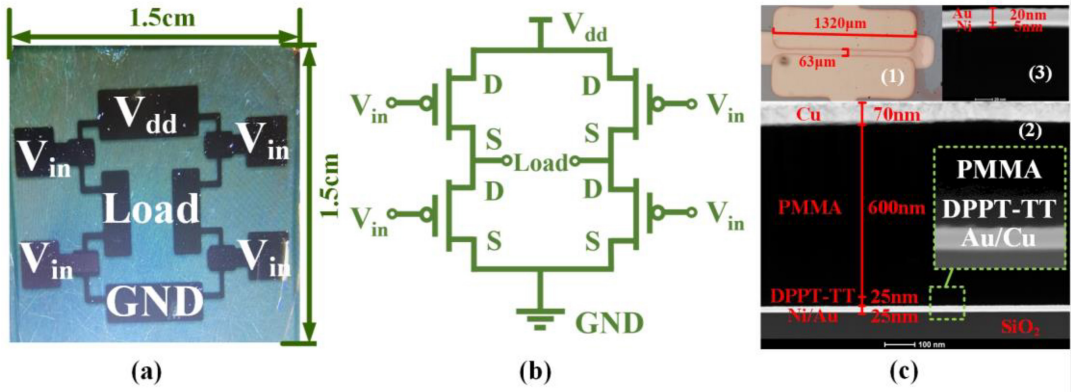


**FIGURE 3.** The substance of the H-bridge circuits. (a) The top view of the fabricated circuit. (b) H-bridge equivalent circuit diagram. (c) Device profiles: (1) Length and width of electrodes by SEM. (2) Cross-sectional TEM. The inset shows the partial view of the decomposition surface between electrode, DPPT-TT and PMMA by TEM. (3) Electrode thickness at high resolution by TEM.

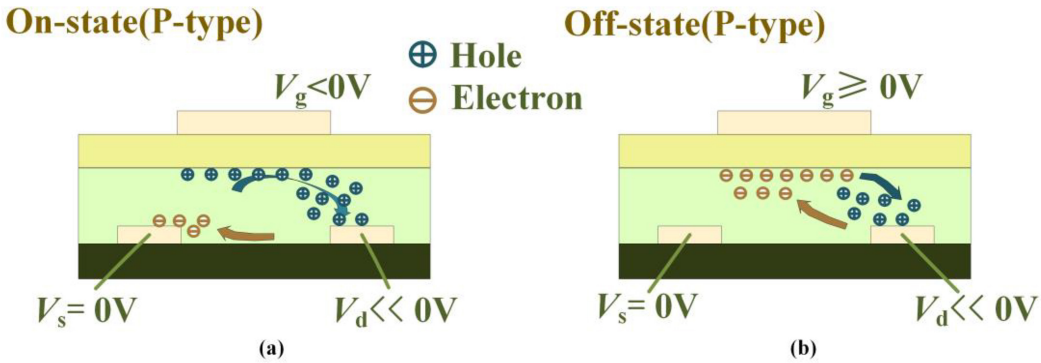


**FIGURE 4.** Schematic representation and operating principle of OFET at (a) On-state as a P-type FET, where mainly dominated by electron and hole drift motion. (b) Off-state as a P-type FET, where most of the electrons and holes are complexed in the channel region.

semiconductor layer (80 °C, 5 min pre-annealing; 150 °C, 1 hour annealing); (3). Fabricating dielectric layer: spin coat a layer of PMMA as the gate insulator layer (80 °C, 2 hour annealing); (4). Fabricating top electrode: deposit a 70 nm Cu layer to realize the Gate electrode(top electrode is also patterned using a metal mask covered onto the substrate).

Four top-gate bottom-contact thin-film(25 nm active layer) OFETs in the H-bridge circuit possess an 63 μm × 1320 μm(length × width) channel, fabricated on a 1.5 cm × 1.5 cm Corning glass substrate. The physical diagram of the manufactured H-bridge circuit is shown in the Fig. 3(a). The equivalent circuit diagram for this H-bridge circuit is showing in the Fig. 3(b).

As shown in Fig. 3(c), a focused ion beam transmission electron microscope(FIB-TEM) is utilized to measure the thickness of each layer. The thickness of semiconductor layer above the electrode is 25 nm and dielectric layer is 600 nm. With a superior interfacial roughness and exceptional thickness uniformity, the structure is clearly visible in each layer.

## III. MECHANISM AND DISCUSSION

Unlike conventional inorganic semiconductor-based field effect transistors, copolymer OSC-based OFETs have a unique transportation characteristic as they possess ambipolar conduction capability, allowing the channel layer to display either N-type or P-type characteristics [8], [9], [10]. Namely, the carrier concentration in the channel region depends on the voltage between the gate and drain voltage of the device. When the voltage applied to the electrodes satisfies $V_{ds} < V_{gs} < 0$, due to the ambipolar conduction capability of copolymer OSCs such as DPPT-TT, a hole channel is formed, and therefore the OFET operates as a P-type FET. Whereas the electrons are being extracted from the channel and pushed to the source electrode ($V_{ds} < 0$), thus creating the electron drift current ($I_n$), as shown in Fig. 4(a). For the off-state case, as shown in Fig. 4(b), when $V_{gs} >> 0 > V_{ds}$, the hole path in the channel region is depleted. Then, electrons and holes can no longer be pushed separately between the source and drain electrodes, resulting in electron-hole complexation directly in the channel region near the drain side. Moreover, due to the presence of electron layer in the channel region of the OFET, the channel region is equivalent to N-type.

For the copolymer OSC-based OFETs, as shown in Fig. 5(a), due to the special characteristics of the current organic materials, which leads to the contact between the metal and the semiconductor can not be ohmic contact, the

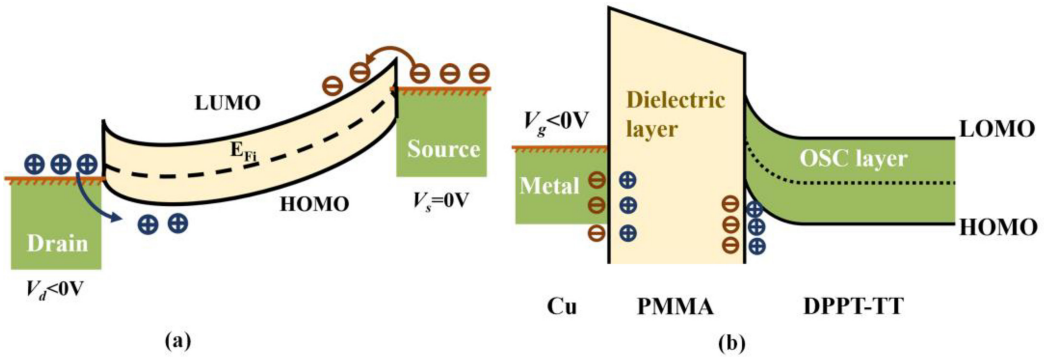


**FIGURE 5.** The energy band diagrams for (a) the Metal-OSC-Metal structure between drain and source electrodes can be equivalent to a lateral back-to-back Schottky junction structure ($V_{ds}$ < 0 V). (b) an accumulation of holes within the semiconductor at a distance from the interface and causes the semiconductors to bend upwards near the dielectric layer. ($V_g$ < 0V, DPPT-TT as a P-type).

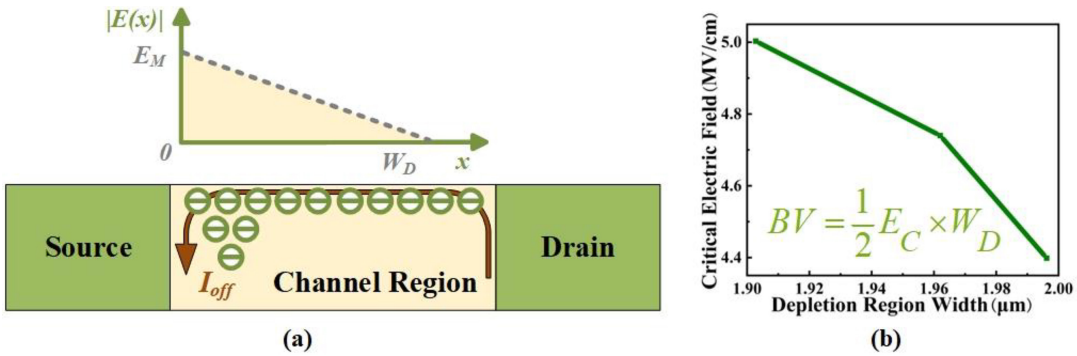


**FIGURE 6.** Operating principle of OFET. (a) A lateral back-to-back Schottky junction structure equivalent and its electric field/band diagram. (b) The critical electric field shows a negative correlation with the width of the depletion zone.

contact between them is Schottky contact forms a typical Schottky junction [7]. Such a Metal-OSC contact satisfies thermal emission(TE) theory that origins from inorganic semiconductor theory as well. Despite using the high-work-function metal of Au, interface dipoles decrease the contact metal's work function, this implies that the thermionic emissions of holes and electrons, at the source and drain, are not severely limited [11]. As shown in Fig. 5(b), when a negative voltage is applied to the gate ($V_{gs} < 0$), an electric field is generated in the device perpendicular to the source-drain direction and directed towards the gate electrode. At the same time, an equal number of charges of opposite polarity are generated on both sides of the dielectric layer, forming a dipole layer. The dielectric layer PMMA is negatively charged near the interface, while the semiconductor OSC is positively charged near the interface. This leads to an accumulation of holes within the semiconductor at a distance from the interface and causes the semiconductors to bend upwards near the dielectric layer. These accumulated holes can then be driven by the source-drain voltage to form a current.

Due to the Schottky contact nature of OSC-Metal contacts, as shown in Fig. 5(a) and 6(a), the Metal-OSC-Metal structure between drain and source electrodes can be equivalent to a lateral back-to-back Schottky junction structure [7]. For a back-to-back Schottky junction, the reverse-biased Schottky junction dominates the overall current flow between two electrodes when the applied voltage is lower than the breakdown voltage of the reverse-biased Schottky junction. Therefore, by applying the 1-D Poisson's equation, the electric field profile $E(x)$ between the source and drain electrodes ought to satisfy:

$$E(x) = -\frac{qN_D}{\varepsilon_S}(W_D - x) \tag{1}$$

where $\varepsilon_s = 3\varepsilon_0$ is the permittivity of DPPT-TT, and the relative permittivity of DPPT-TT is 3 [7], [12]. The $\varepsilon_0 = 8.854 \times 10^{-12}$ F/m is the permittivity of a vacuum. Meanwhile, $N_D$ is the net carrier concentration of the copolymer OSC layer. The depletion width in the OSC layer $W_D$ and breakdown voltage(BV) of the Schottky junction can be therefore obtained, respectively:

$$W_D = \sqrt{\frac{2\varepsilon_S BV}{qN_D}} \tag{2}$$

$$BV = \frac{E_C W_D}{2} \tag{3}$$

Clearly, the avalanche-like breakdown of the copolymer OSC occurs when the electric field peak reaches the critical electric field ($E_C$) of DPPT-TT at the interface between metal and OSC($x = 0$). As shown in Fig. 6(b), same as that in inorganic semiconductor cases, the critical electric field

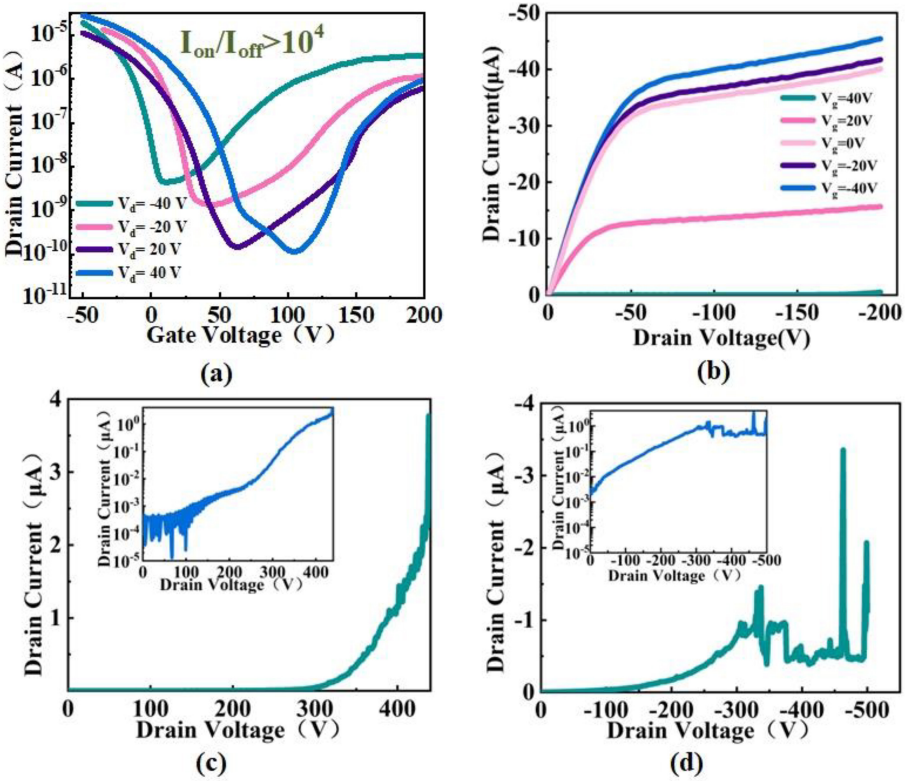


**FIGURE 7.** Experimentally measured OFET. (a) Transfer characteristic curves in log coordinates. (b) On-state output characteristic curve of the devices operate as a P-type. (c) Off-state BV curve when the devices operate as a N-type. The inset shows BV curve in log coordinates. (d) Off-state BV curve when the devices operate as a P-type. The inset shows BV curve in log coordinates.

shows a negative correlation with the width of the depletion region.

As shown in Fig. 7(a), the on/off ratio of the fabricated thin-film OFET reaches $10^4$ reflecting the fabricated OFET's strong ability to regulate current. Such a high on/off ratio meets or even exceeds the state-of-the-art OFETs based on DPPT-TT [13]. The on/off ratio of the fabricated OFETs is mainly limited by the nature of DPPT-TT. For a higher on/off ratio of OFETs, one is expected to employ other OSCs such as N2200 [13], [14], [15], [16]. Moreover, the threshold voltage of the fabricated OFETs is 5 V, which provides a favorable operating condition for the usage of OFETs in the H-bridge circuits. It is worthy to be noted that the commonly used linear extrapolation method is employed [17], [18]. The voltage drop between the semiconductor layer and the source-drain metal causes the extracted mobility to be affected by the magnitude of the drain voltage, which can be reduced by choosing to extract the mobility in the saturation region. Then $I_{\mathrm{Dsat}}$ ought to satisfy:

$$I_{\mathrm{Dsat}} = \frac{W}{2L}\mu_{\mathrm{sat}}C_i\left(V_{\mathrm{gs}} - V_T\right)^2 \tag{4}$$

where $I_{\mathrm{Dsat}}$ is the drain current in the saturation region, $W$ is the channel length, $L$ is the channel width, $\mu_{\mathrm{sat}}$ is the mobility to be determined, $C_{\mathrm{i}}$ is dielectric capacitance per unit area, $V_{\mathrm{gs}}$ is the voltage applied across gate to source electrode and $V_{\mathrm{T}}$ is the threshold voltage can be determined from the transfer curve.

$$\sqrt{I_{\mathrm{Dsat}}} = \sqrt{\frac{W}{2L}\mu_{\mathrm{sat}}C_i}\left(V_{\mathrm{gs}} - V_T\right) \tag{5}$$

For simplicity, we assume the mobility of electron and hole are the same. Therefore, the mobility $\mu_{\mathrm{sat}}$ ought to satisfy:

$$\mu_{\mathrm{sat}} = \left(\frac{\partial\sqrt{I_{\mathrm{D}}}}{\partial V_{\mathrm{gs}}}\right)^2 \frac{2L}{WC_{\mathrm{i}}} \tag{6}$$

By using Eq. (6), the mobility of the fabricated OFETs can be extracted as 0.22 cm$^2$/(V·s), which is consistent with reported results [8]. Note that the mobility extracted from fabricated devices is predominantly dictated by the material itself, thus resulting in DPPT-TT exhibiting higher mobility than N2200 but lower than C8-BT/PS and TIPS-pentacene/PS [13], [14], [15]. Meanwhile, as shown in Fig. 7(b), the $I_{\mathrm{d}}$-$V_{\mathrm{d}}$ characteristics of fabricated OFETs are still consistent with conventional FETs.

Fig. 7(c) and (d) show the measured breakdown voltage of OFET when it operates as N-type or P-type respectively. Although the copolymer OSCs possess no classic single crystal structure and therefore have no commonly understood impact ionization process, the distinctive avalanche-like breakdown mechanism of the copolymer OSCs provides a high critical electric field (>5 MV/cm) and astonishing electric breakdown performance [6]. The measured off-state breakdown voltage of the fabricated copolymer OSC-based

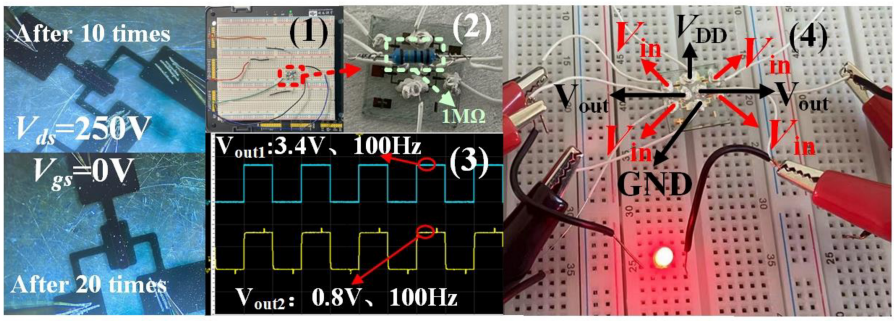


**FIGURE 8.** (a) Circuit surface after repeated testing(10 times and 20 times, interval>1 min, within 48hours). (b) Experimentally measured circuit: (1) Breadboard used for testing Connect a 1 MΩ resistor in series with the output ($V_{dd}$ = 5 V, $V_{in}$ (0 V ~ 5 V)). (2) A 1 MΩ resistor employed as the output load. (3) The output waveform at both ends of the resistor. (4) The LED is driven after applying square wave signal to the $V_{in}$(−5 V~5 V).

OFET excesses 300 V as it operates N or P type. As shown in Fig. 6(a), when the OFET operates off-state, the reverse-biased Schottky junction between the drain and source sustains the majority of the applied voltage [6], [7]. In this work, the off-state BV is determined by the externally applied drain voltage when an uncontrolled leaking current occurs (Current density $J_{off} >> 10^{-9}$ A/μm).

As Fig. 8(a) intuitively shows, it is remarkable that the cyclic BV tests(over 20 times, within 48 hours) were undertaken without obvious structural damage to the device, which indicates the recoverability of the non-destructive and repeatable avalanche-like breakdown. As for the on-state performance, considering the fact that the active layer thickness of the fabricated OFETs is only 25 nm, the transmission of charge can be simplified as only occurs in the lateral direction between two electrodes. Therefore, the current density of each the fabricated OFET can be obtained by using the saturation current($I$) and cross-sectional area ($S = 25$ nm $\times$ 1320 μm). Therefore, the current density of the single OFET is $J = I/S$. For a typical on-state operation case, the saturation current is 40 μA ($|V_{ds}| = 70$ V, $|V_{gs}| = 40$ V, P-type), therefore the current density reaches more than 121 A/cm$^2$. Furthermore, an H-bridge circuit is also been fabricated to demonstrate the feasibility of the copolymer OSC-based power devices in forming the power management integrated circuits. As shown in Fig. 8(b), in order to avoid the dead time, the input signal is only applied in one direction of the H-bridge circuit [19], [20], [21]. To further demonstrate the drive performance of the OSC-based H-bridge circuit, a 1 MΩ resistor and an LED lamp are employed as the output load separately. As shown in Fig. 8(b)(3), the measured results indicate that output voltage reaches 2.6 V with $V_{dd} = 5$ V when 1 MΩ resistor is employed.

## IV. CONCLUSION

In this paper, to explore the on- and off-state performance of copolymer OSC-based lateral OFETs in its applications in the future power realm, an H-bridge circuit based on the OFET with the top-gate bottom-contact structure is proposed and fabricated. By using thin-film copolymer OSC-based OFET, the measurements indicate that the fabricated devices can achieve a high current density(above 121 A/cm$^2$) and a high on-off current ratio(above $10^4$). When the OFETs operate off-state, the reverse-biased Schottky junction is sustaining the majority of the applied voltage between the Drain and Source.

The non-destructive avalanche-like breakdown mechanism provides the OFET with a 300 V high BV. By employing square wave signal (−5 V~5 V) as the $V_{in}$, the H-bridge circuit can properly drive an LED lamp. Due to the advantages in reliability and simplicity of the spin-coating process-based fabrication technique, it is expected that the copolymer OSC-based OFETs can be a promising building block for future power applications.

## REFERENCES

[1] E. C. P. Smits et al., "Bottom-up organic integrated circuits," *Nature*, vol. 455, pp. 956–959, Oct. 2008, doi: 10.1038/nature07320.
[2] W. Huang and A. Facchetti, "Organic circuits reach new heights," *Nat. Electron.*, vol. 4, pp. 544–545, Aug. 2021, doi: 10.1038/s41928-021-00634-5.
[3] T. P. Nguyen et al., "Polypeptide organic radical batteries," *Nature*, vol. 593, no. 7857, pp. 61–66, May 2021, doi: 10.1038/s41586-021-03399-1.
[4] S. Chung and T. Lee, "Towards flexible CMOS circuits," *Nat. Nanotechnol.*, vol. 15, pp. 11–12, Jan. 2020, doi: 10.1038/s41565-019-0596-6.
[5] B. Crone et al., "Large-scale complementary integrated circuits based on organic transistors," *Nature*, vol. 403, pp. 521–523, Feb. 2000, doi: 10.1038/35000530.
[6] J. Zhang et al., "A 2.2kV organic semiconductor- based lateral power device," *IEEE Electron Device Lett.*, vol. 43, no. 2, pp. 276–279, Feb. 2022, doi: 10.1109/LED.2021.3135699.
[7] J. Zhang et al., "Avalanche-like breakdown behavior of copolymer organic semiconductor-based Schottky junction structure," *Appl. Phys. Lett.*, vol. 121, no. 12, Sep. 2022, Art. no. 123502, doi: 10.1063/5.0104970.
[8] C. Liu et al., "Revealing charge transport and device operations of organic ambipolar transistors and inverters by four-probe measurement," *Adv. Electron. Mater.*, vol. 7, no. 3, Mar. 2021, Art. no. 2001134, doi: 10.1002/aelm.202001134.
[9] Z. Qin, K. Kuribara, Y. Ogasahara, and T. Sato, "Hybrid CMOS and pseudo-CMOS organic memory for flexible sensors," *IEEE Sensors J.*, vol. 23, no. 20, pp. 24050–24059, Oct. 2022, doi: 10.1109/JSEN.2022.3153714.

[10] Z. Chen et al., "High-performance ambipolar diketopyrrolopyrrole-thieno [3,2-b]thiophene copolymer field-effect transistors with balanced hole and electron mobilities," *Adv. Mater.*, vol. 24, no. 5, pp. 647–652, Feb. 2012, doi: 10.1002/adma.201102786.

[11] Y. Xu, H. Sun, E.-Y. Shin, Y.-F. Lin, W. Li, and Y.-Y. Noh, "Planar-processed polymer transistors," *Adv. Mater.*, vol. 28, no. 38, pp. 8531–8537, Oct. 2016, doi: 10.1002/adma.201601589.

[12] M. P. Hughes, K. D. Rosenthal, N. A. Ran, M. Seifrid, G. C. Bazan, and T.-Q. Nguyen, "Determining the dielectric constants of organic photovoltaic materials using impedance spectroscopy," *Adv. Functional Mater.*, vol. 28, no. 32, p. 1801542, Aug. 2018, doi: 10.1002/adfm.201801542.

[13] F. Huang, Y. Xu, Z. Pan, W. Li, and J. Chu, "Direct patterning on top-gate organic thin-film transistors: improvement of on/off ratio, subthreshold swing, and uniformity," *IEEE Electron Device Lett.*, vol. 41, no. 7, pp. 1082–1085, Jul. 2020, doi: 10.1109/LED.2020.2998820.

[14] C. Jiang, H. W. Choi, X. Cheng, H. Ma, D. Hasko, and A. Nathan, "Printed subthreshold organic transistors operating at high gain and ultralow power," *Science*, vol. 363, no. 6428, pp. 719–723, Feb. 2019, doi: 10.1126/science.aav7057.

[15] L. Feng et al., "Unencapsulated air-stable organic field effect transistor by all solution processes for low power vapor sensing," *Sci. Rep.*, vol. 6, p. 20671, Feb. 2016, doi: 10.1038/srep20671.

[16] J. Zhao, W. Tang, Q. Li, W. Liu, and X. Guo, "Fully solution processed bottom-gate organic field-effect transistor with steep subthreshold swing approaching the theoretical limit," *IEEE Electron Device Lett.*, vol. 38, no. 10, pp. 1465–1468, Oct. 2017, doi: 10.1109/LED.2017.2742952.

[17] Z. Bai et al., "Comparative study on extraction methods of threshold voltage for thin–film transistors," *J. Soc. Info. Display*, vol. 27, no. 12, pp. 816–821, Dec. 2019, doi: 10.1002/jsid.831.

[18] R. Nirosha and R. Agarwal, "Characterization and modeling of threshold voltage for organic and amorphous thin-film transistors," *Microelectronics Reliab.*, vol. 147, Aug. 2023, Art. no. 115054, doi: 10.1016/j.microrel.2023.115054.

[19] A. Mora, J. Juliet, A. Santander, and P. Lezana, "Dead-time and semiconductor voltage drop compensation for cascaded H-bridge converters," *IEEE Trans. Ind. Electron.*, vol. 63, no. 12, pp. 7833–7842, Dec. 2016, doi: 10.1109/TIE.2016.2563378.

[20] D. Zammit, M. Apap, and C. S. Staines, "Dead time compensation in H-bridge inverters," *Int. J. Ind. Electron. Drives*, vol. 4, no. 1, pp. 56–68, Jan. 2018, doi: 10.1504/IJIED.2018.090411.

[21] B. Li et al., "A new model-based dead-time compensation strategy for cascaded H-bridge converters," *IEEE Trans. Ind. Electron.*, vol. 70, no. 4, pp. 3793–3802, Apr. 2023, doi: 10.1109/TIE.2022.3177757.